International Journal of Solids and Structures 46 (2009) 3441–3450

Contents lists available at ScienceDirect

International Journal of Solids and Structures

journal homepage: www.elsevier.com/locate/ijsolstr

Numerical analysis of an electrode embedded between dissimilar electrostrictive materials

Y.H. Kim, H.G. Beom *

Department of Mechanical Engineering, Inha University, 253 Yonghyun-dong, Incheon 402-751, Republic of Korea

ARTICLE INFO

Article history:
Received 21 October 2008
Received in revised form 20 April 2009
Available online 27 May 2009

Keywords:
Electrostrictive material
Electrode
Stress intensity factor
Finite element analysis

ABSTRACT

The asymptotic problem of an electrode that is embedded between dissimilar electrostrictive materials and subjected to electric loading is numerically analyzed by using the finite element method. Electrostatic analysis for the asymptotic problem is conducted under the small-scale saturation condition on the basis of the mathematical equivalence between anti-plane shearing and electrostatics. The distribution of the electric displacement fields is obtained. It is shown that the shapes of the saturation zones are affected by the ratios of the permittivities and the saturated electric displacements between the dissimilar electrostrictive materials. Stress fields that are generated for matching incompatible strains, which are induced by non-uniform electric displacement fields, are numerically calculated for various combinations of the material properties. Also, stress intensity factors for arbitrary small cracks that are initiated from the edge of an electrode are evaluated. Behaviors of cracking that may take place at the edge of an electrode are discussed.

1. Introduction

Electrostrictive materials embedded an internal electrode are the structure commonly observed in ceramic multilayer actuators. In this structure of an actuator, an unavoidable problem is that the strong stress fields near the edge of an electrode are generated due to the mismatch of electrostrictive strains that are induced by electric displacements. These intensified stress fields fracture electrostrictive ceramics with great brittleness (Aburatani et al., 1994; Winzer et al., 1989; Beom, 1999). This crack problem of electrostrictive materials with an internal electrode has attracted considerable attention of researchers who investigate the reliability and durability of electrostrictive actuators. Yang and Suo (1994) obtained the stress fields by analyzing the asymptotic problem of an internal electrode in electrostrictive actuators through the linear dielectric model and complex function theory. They also examined the micro-cracking of a ceramic that may occur ahead of an electrode edge. Hao et al. (1996) proposed the perfect saturation model, and using it they theoretically investigated the electrostrictive material with an internal electrode under the small-scale saturation condition. Beom and Atluri (2003) examined the effects of electric fields on the cracking behavior of ferroelectric material on the basis of the perfect saturation model and the domain switching model. The electrical fields and the elastic fields near the edge of the internal electrode in a ceramic multilayer actuator are numerically calculated by using the finite element method (Gong and Suo, 1996; Hom and Shankar, 1996). Ru et al. (1998) derived the formulation that can directly calculate the stress intensity factor of the crack tip in electrostrictive materials without solving the boundary value problem. Beom et al. (2006) investigated the influence of the transverse electric displacement on fracture behavior of the electrostrictive materials. The modified boundary-layer analysis for an electrostrictive material with an electrode layer was also carried out under the small-scale saturation condition (Beom et al., 2008). Li and Chen (2007) analyzed the semi-permeable interface crack between dissimilar piezoelectric materials. Also, Li and Chen (2008) studied the semi-permeable interface crack in a dielectric/piezoelectric bimaterial. In their works, it is shown that the combination of dissimilar materials dominates the singularity of the near-tip fields. Until now, most studies of the crack problems of electrostrictive materials have been concentrated on the case when the material is homogeneous. However, the crack problem of dissimilar electrostrictive materials with an electrode has not been studied yet.

In this paper, the asymptotic problem of dissimilar electrostrictive materials with an internal electrode is numerically analyzed using the finite element method under the small-scale saturation condition. Electrostrictive materials electrically obey the electric displacement saturation model are mechanically linear-elastic. First, numerical results of electric displacement fields are obtained through electrostatic analysis on the basis of the mathematical equivalence between anti-plane deformation and electricity. It is shown that the size and shape of saturation zones are dependent

* Corresponding author. Tel.: +82 32 860 7310; fax: +82 32 868 1716.
E-mail address: hgbeom@inha.ac.kr (H.G. Beom).

0020-7683/$ - see front matter © 2009 Elsevier Ltd. All rights reserved.
doi:10.1016/j.ijsolstr.2009.05.012

on the ratios of the permittivitties and the saturated electric displacements. Next, the stress fields that are induced by the non-uniform electric displacement fields are numerically calculated. Finally, the stress intensity factors of the tip of an arbitrarily small crack that is initiated from the edge of an internal electrode are systemically evaluated for various combinations of the material properties of dissimilar electrostrictive materials. The effects of electric, elastic, and electrostrictive properties on the behavior of the cracking are also demonstrated.

2. Asymptotic problem

An electrostrictive material is mechanically linear-elastic and, due to the electrostriction effect, experiences a deformation under electric loading that is proportional to the square of the electric displacement field. Even if the electrostrictive material is not subjected to mechanical loading, the self-equilibrated stress fields will be generated by the incompatible electrostrictive strain that is induced by non-uniform electric displacement fields if the electric fields are applied. Similar to the case of elastic materials under thermal loading, the Hook's law of electrostrictive materials under the plane strain condition yields

$$\begin{aligned}
\sigma_{11} &= \frac{Y}{(1+\nu)(1-2\nu)}[\nu\gamma_{22}+(1-\nu)\gamma_{11}] \\
&\quad - \frac{YQ}{(1+\nu)(1-2\nu)}\left[(\nu-q)D_2^2+(1-2q\nu-\nu)D_1^2\right], \\
\sigma_{22} &= \frac{Y}{(1+\nu)(1-2\nu)}[\nu\gamma_{11}+(1-\nu)\gamma_{22}] \\
&\quad - \frac{YQ}{(1+\nu)(1-2\nu)}\left[(\nu-q)D_1^2+(1-2q\nu-\nu)D_2^2\right], \\
\sigma_{12} &= \frac{Y}{(1+\nu)}\gamma_{12} - \frac{YQ(1+q)}{(1+\nu)}D_1D_2, \\
\sigma_{33} &= \nu(\sigma_{11}+\sigma_{22}) + YQq\left(D_1^2+D_2^2\right).
\end{aligned} \tag{1}$$

Here, σ_{ij} is the stress tensor that is composed of a mechanical portion and an electrostrictive portion. γ_{ij} is the strain tensor. D_i is the electric displacement vector. Subscripts in a letter denote the components of the Cartesian coordinates. Y and ν are the Young's modulus and the Poisson's ratio, respectively. Q and q are the electrostriction coefficients of the two dissimilar materials.

Since the influence of stress fields on electric fields is very small in typical electrostrictive materials, the electro-mechanical coupling of electrostrictive materials can be ignored (Yang and Suo, 1994). Thus, we assume that the electric displacement fields are the function of only the electric fields. We employ the electric displacement saturation model in describing the electrical nonlinearity or of electrostrictive materials. For the case of electrostrictive materials, Hao et al. (1996) first introduced the electric displacement saturation model into examining the singular behavior of stress fields near the edge of an internal electrode embedded in a ceramic actuator. Gao et al. (1997) proposed the strip saturation model, which are generalized from the classical Dugdale model, for describing the electrical nonlinear zone near the crack tip in a piezoelectric ceramic. They derived the energy release rate for the electrically yielded finite crack in a piezoelectric ceramic. As indicated by Beom et al. (2008), the difference between the polarization saturation model and the electric displacement saturation model is nearly indistinguishable for typical electrostrictive materials. In analyzing the problem, we will utilize the electric displacement saturation model given by

$$\begin{aligned}
&D_i = \varepsilon E_i \quad \text{for } E < E_0, \\
&D = D_0 \quad \text{for } E > E_0.
\end{aligned} \tag{2}$$

Here, E_i is the electric field vector. D and E denote the magnitudes of the electric displacement vector and the electric field vector, which are defined as $D = \sqrt{D_iD_i}$ and $E = \sqrt{E_iE_i}$, respectively. The repetition of an index in a term denotes the summation with respect to that index over its range, i.e., 1–2. $\varepsilon = D_0/E_0$ is the permittivity of a dielectric material. D_0 is the saturated electric displacement of electrostrictive materials that is experimentally measured under an uni-axial electric field. E_0 is the yield electric field, i.e., the value of an electric field at the onset of the saturation of the electric displacement.

Consider the asymptotic problem of a semi-infinite electrode that is embedded between dissimilar electrostrictive materials and subjected to electric loading as shown in Fig. 1. Dissimilar electrostrictive materials are perfectly bonded with each other on the interface of the positive x_1-axis. The thin electrode lies on the negative x_1-axis along the interface of the dissimilar electrostrictive materials. Since the thickness of an electrode progressively decreases to zero, the electric displacement field in the direction of x_2 and the electric potential across the electrode are continuous. Assuming that the small-scale saturation condition holds, the remote electric displacement fields at infinity are assumed to be the near-tip fields given by

$$\begin{aligned}
&D_2+iD_1 = \frac{iK_D^{(1)}}{\sqrt{2\pi z}} \quad \text{as } z\to\infty, \text{ for material 1, and} \\
&D_2+iD_1 = \frac{iK_D^{(2)}}{\sqrt{2\pi z}} \quad \text{as } z\to\infty, \text{ for material 2.}
\end{aligned} \tag{3}$$

Here, the superscripts (1) and (2) denote the two materials. $K_D^{(1)}$ and $K_D^{(2)}$ are the intensity factors of the electric displacement fields of materials 1 and 2, respectively. We can obtain the relationship, $K_D^0 = K_D^{(1)}/\varepsilon^{(1)} = K_D^{(2)}/\varepsilon^{(2)}$, from the condition of the continuity of the electric potential across the interface of $x_1 > 0$. z is the complex variable defined as $z = x_1 + ix_2$. Here, we introduce the cylindrical coordinates (r,θ) with the origin located at the crack tip. The electric potential along the electrode is assumed to be zero. Also the stress fields and the displacement are continuous across the electrode. Therefore, the electrode has the condition given by

$$\begin{aligned}
&\phi(r,\pm\pi) = 0, \\
&\sigma_{ij}(r,\pi) = \sigma_{ij}(r,-\pi), \quad u_i(r,\pi) = u_i(r,-\pi).
\end{aligned} \tag{4}$$

If the body force per unit volume and the free charge density do not exist at each point in the material, the Gauss law and the equilibrium law are, respectively,

$$D_{i,i} = 0, \tag{5}$$

$$\sigma_{ij,j} = 0. \tag{6}$$

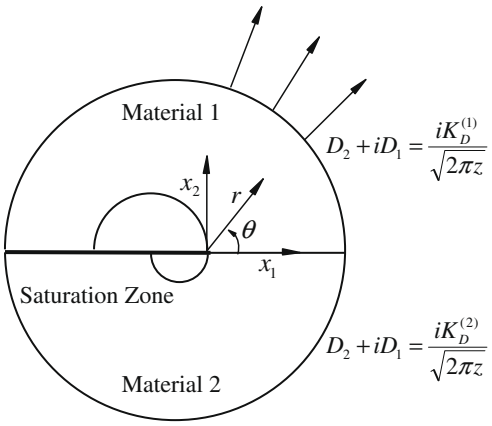

Fig. 1. Asymptotic problem.

Once the distribution of electric displacement fields is determined by Eqs. (2)–(5), we can obtain the stress fields that satisfy conditions (1) and (6). Instead of solving the complex boundary value problem, we will analyze the asymptotic problem by using the finite element method.

3. Electrostatic analysis

To find the distribution of electric displacement fields in dissimilar electrostrictive materials with an electrode lying on their interface, we carry out electrostatic analysis for the asymptotic problem by using the finite element method. The mathematical equivalence of the governing equations and the physical quantities between electricity and anti-plane deformation is well-known. That is, the electric potential, the electric fields, and the electric displacement fields are mathematically equal to the anti-plane displacement, the anti-plane shear strain, and the anti-plane shear stress, respectively. Likewise, the electric displacement saturation model can be replaced by the elastic-perfectly plastic model that is used in solid mechanics. The electrode problem can be regard as the anti-plane problem for the rigid sheet. Thus, we actually perform the numerical analysis of the anti-plane rigid sheet problem instead of solving the electrostatic problem for the electrode. For convenience, the terms referred in this paper are physical quantities of electricity. The commercial finite element code ABAQUS is utilized in the electrostatic analysis. Each element is the three-dimensional 8-node element C3D8R of the ABAQUS element library. 7200 elements that are arrayed only in the one-layer are used in the analysis. For assuring the accuracy of the electrostatic analysis, the remote field at infinity is assumed to be the near-tip field of the electric potential instead of the electric displacement field.

$$\phi = \mathrm{Im}\left[K_D^0\sqrt{\frac{2z}{\pi}}\right]. \tag{7}$$

From dimensional considerations, the electric displacement fields in dissimilar electrostrictive materials can be expressed as

$$D_i = D_0^{(1)}\tilde{D}_i\left(\frac{r}{r_0^{(1)}}, \theta; \lambda, k\right). \tag{8}$$

Here, tilde ($\sim$) denotes the dimensionless quantity. The dimensionless parameters, λ and k, are the ratios of the saturated electric displacements and the permittivities of material 2 to material 1, and are given by $\lambda = D_0^{(2)}/D_0^{(1)}$ and $k = \varepsilon^{(2)}/\varepsilon^{(1)}$, respectively.

We perform finite element analysis for various combinations of the dimensionless parameters, λ and k. Even if k is only two times

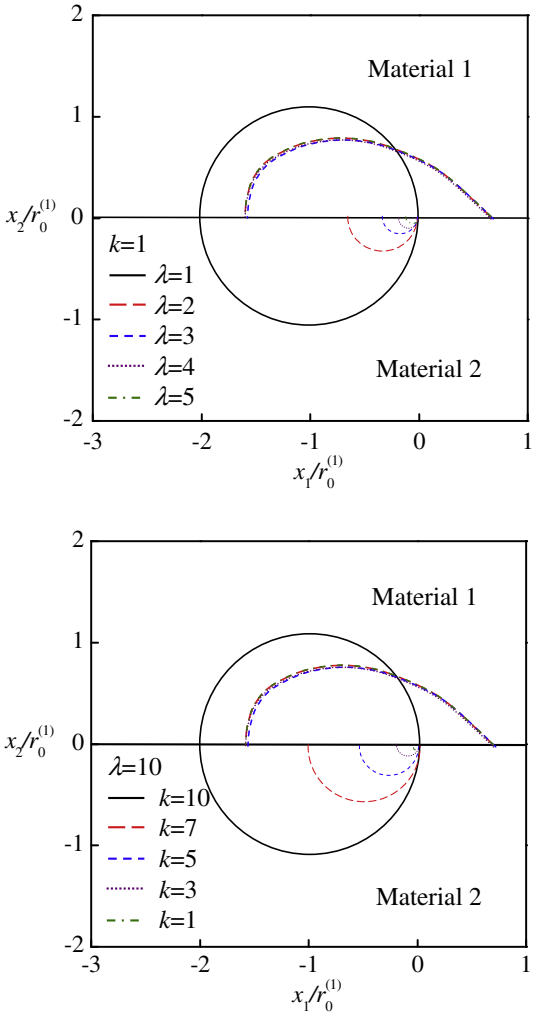

Fig. 2. Variation of saturation zones with λ.

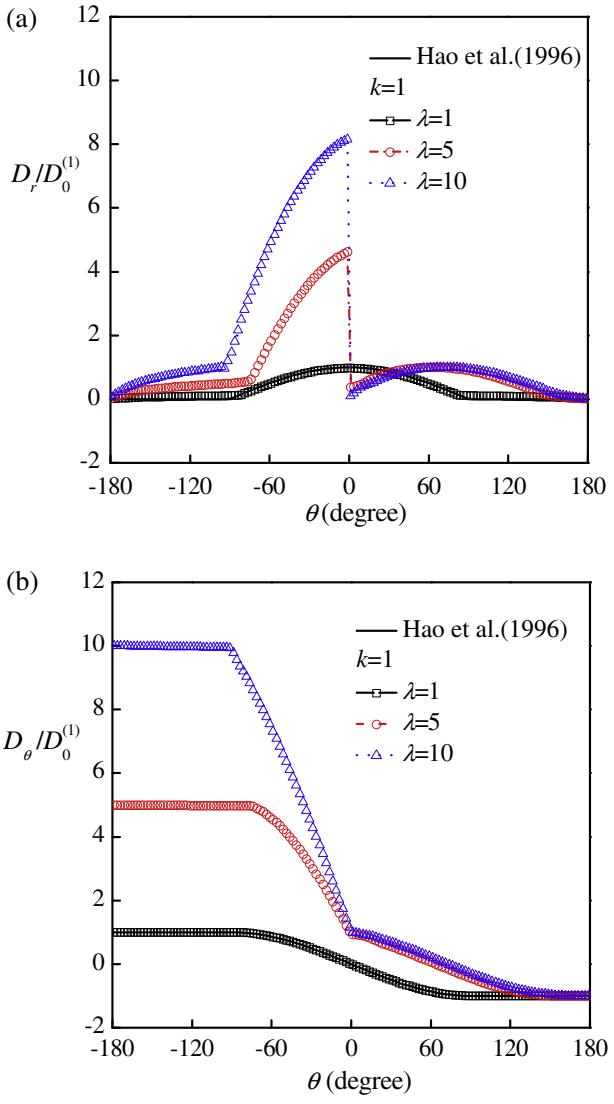

Fig. 3. Normalized electric displacement fields at the distance $r/r_0^{(1)} \approx 0.01$ from the crack tip, as a function of θ for various λ when $k = 1$. (a) Radial component. (b) Tangential component.

greater than λ, the small-scale saturation condition is not satisfied because the saturation zone becomes large enough to swallow the large portion of the linear dielectric zone outside the saturation boundary. Thus, we restrict our attention to the case when $k < \lambda$. Fig. 2 illustrates that the shape of the saturation zone in the vicinity of the edge of the electrode is circular with a radius of $r_0^{(1)} = K_D^2 \Big/ \left[2\pi\left(D_0^{(1)}\right)^2\right]$ for the case of homogeneous electrostrictive materials ($k = \lambda = 1$). For the case when $k = 1$, the larger is λ, the smaller is the semi-circular saturation zone in material 2. Further, the shape and size of the saturation zone in material 1 do not change even though λ changes. For the case when $\lambda = 10$, the radius of the semi-circular saturation zone in material 2 decreases rapidly as k increases. Furthermore, the shape and size of the saturation zone in material 1 do not change. It is noted that the saturation zone in material 1 maintains a regular size and shape for all combinations of k and λ in this analysis.

The cylindrical component of the electric displacement field at the distance $r/r_0^{(1)} = 0.01$ from the edge of an electrode is plotted as a function of θ for various combinations of k and λ in Figs. 3 and 4. For the case of homogeneous materials ($\lambda = k = 1$), the numerical result agrees well with the analytic solution of Hao et al. (1996).

4. Elastic analysis

The elastic analysis for the asymptotic problem of an internal electrode between dissimilar electrostrictive materials is numerically conducted by using the finite element method. The electrostrictive strains that are induced by the non-uniform electric displacement fields are incompatible. Thus, the self-equilibrated stress fields are generated to match the incompatible electrostrictive strains. Once the electrostrictive portion σ_{ij}^E of the Hook's law is determined from the numerical results of the electric displacement fields that are calculated in the previous section, the self-equilibrated stress fields that satisfy the equilibrium equation can be evaluated. The mesh and geometry of the finite element model should be consistent with those of Section 3 in the in-plane view. The four-node plane strain reduced element CPE4R in the ABAQUS element library is used. The number of elements is 7200. The electrostrictive portion of Eq. (1) at the Gaussian point of the CPE4R element can be calculated by substituting the numer-

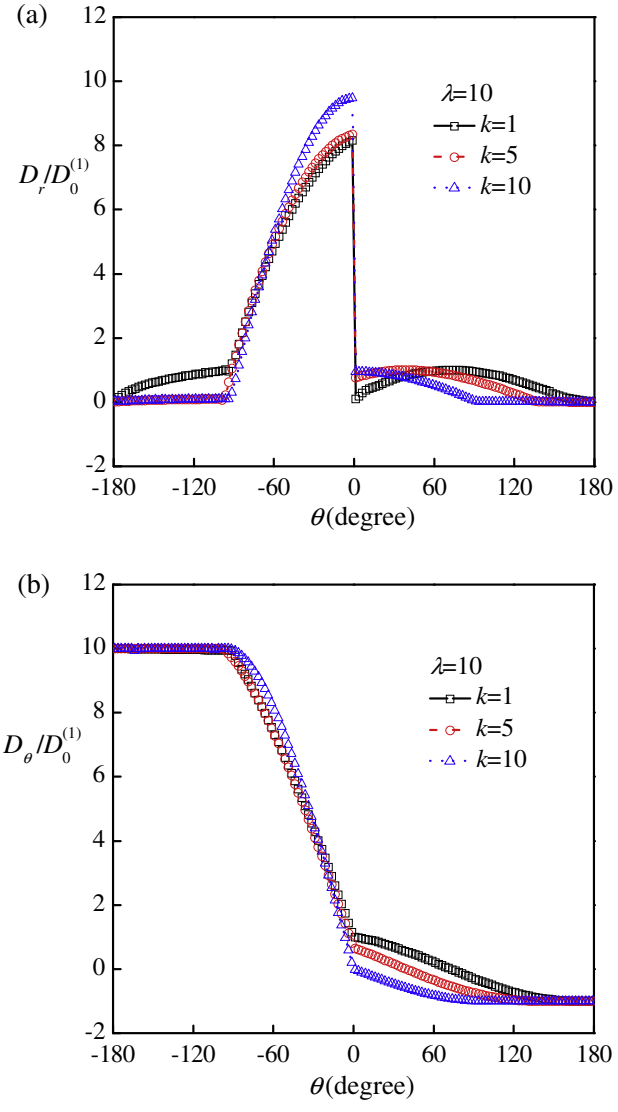

Fig. 4. Normalized electric displacement fields at the distance $r/r_0^{(1)} \approx 0.01$ from the crack tip, as a function of θ for various k when $\lambda = 1$. (a) Radial component. (b) Tangential component.

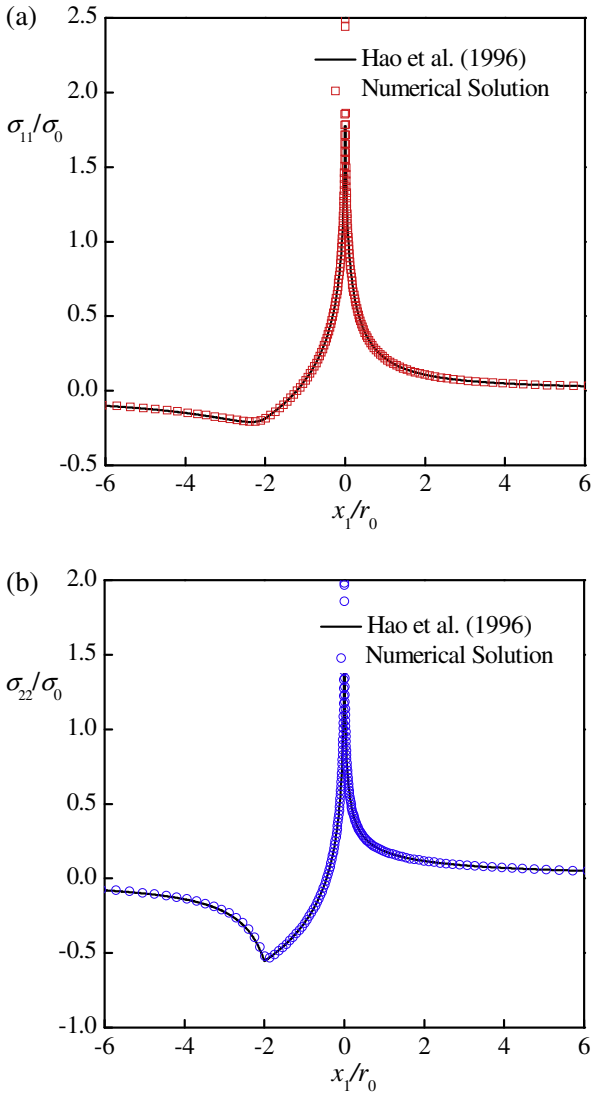

Fig. 5. Comparison of the result of finite element analysis and the analytic solution for a homogeneous, electrostrictive material.

ical data of the electric displacement fields at the Gaussian points of the C3D8R elements into the following equation:

$$\sigma_{11}^{E(p)} = -\frac{Y^{(p)}Q^{(p)}}{(1+\nu^{(p)})(1-2\nu^{(p)})}\left[(\nu^{(p)}-q^{(p)})D_2^2+(1-2q^{(p)}\nu^{(p)}-\nu^{(p)})D_1^2\right],$$
$$\sigma_{22}^{E(p)} = -\frac{Y^{(p)}Q^{(p)}}{(1+\nu^{(p)})(1-2\nu^{(p)})}\left[(\nu^{(p)}-q^{(p)})D_1^2+(1-2q^{(p)}\nu^{(p)}-\nu^{(p)})D_2^2\right],$$
$$\sigma_{12}^{E(p)} = -\frac{Y^{(p)}Q^{(p)}(1+q^{(p)})}{(1+\nu^{(p)})}D_1^{(p)}D_2^{(p)}. \tag{9}$$

Here, p in the superscript is $p = 1$ and 2 for the material (1) and (2), respectively. Subsequently, by introducing the electrostrictive stress σ_{ij}^{E} as the initial stress fields in the finite element analysis, we can obtain the stress fields. Through dimensional analysis, the stress fields in dissimilar electrostrictive materials can be normalized as

$$\sigma_{ij} = \sigma_0^{(1)}\tilde{\sigma}_{ij}\left(\frac{r}{r_0^{(1)}}, \theta; k, \lambda, m, n, \nu^{(1)}, \nu^{(2)}, q^{(1)}, q^{(2)}\right). \tag{10}$$

In Eq. (10), $\sigma_0^{(1)} = Y^{(1)}Q^{(1)}\left(D_0^{(1)}\right)^2$, $m = Y^{(2)}/Y^{(1)}$, and $n = Q^{(2)}/Q^{(1)}$. For the case when the material is homogeneous, the reference length and the reference stress are $r_0 = K_D^2/(2\pi D_0^2)$ and $\sigma_0 = YQD_0^2$, respectively. The stress fields are affected by the ratios of the electrical, elastic, and electrostrictive properties between the dissimilar electrostrictive materials. Our attention is restricted to the effects of the dimensionless parameters k, λ, m, and n on the stress fields. We assume that $\nu^{(1)} = \nu^{(2)} = \nu$ and $q^{(1)} = q^{(2)} = q$. The Poisson's ratio and the electrostrictive coefficient of the typical electrostrictive materials used in this analysis are $\nu = 0.26$ and $q = 0.38$, respectively. The dimensionless form of the stress fields can be rewritten as

$$\sigma_{ij} = \sigma_0^{(1)}\tilde{\sigma}_{ij}\left(\frac{r}{r_0^{(1)}}, \theta; k, \lambda, m, n, \nu, q\right). \tag{11}$$

The numerical solution of the stress fields for a homogeneous electrostrictive material ($k = \lambda = m = n = 1$) agrees well with the analytic solution of Hao et al. (1996), as shown in Fig. 5. Hao et al. (1996) showed that the singular stress fields near the edge

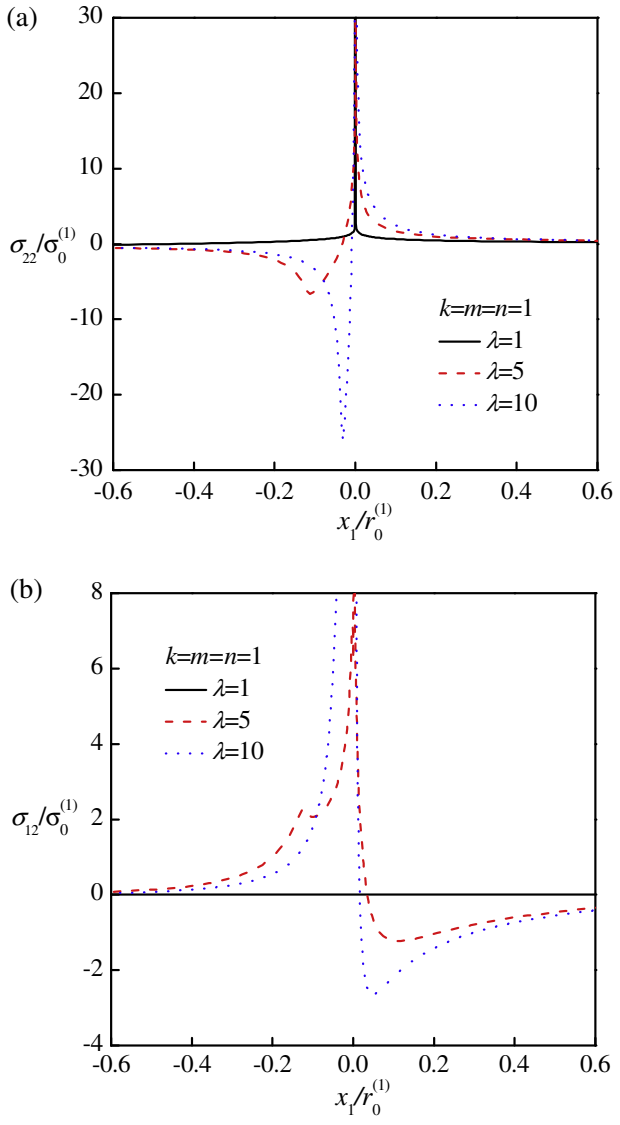

Fig. 6. The variation of normalized stress fields with λ for the case of $k = m = n = 1$. (a) Normal stress σ_{22}. (b) Shear stress σ_{12}.

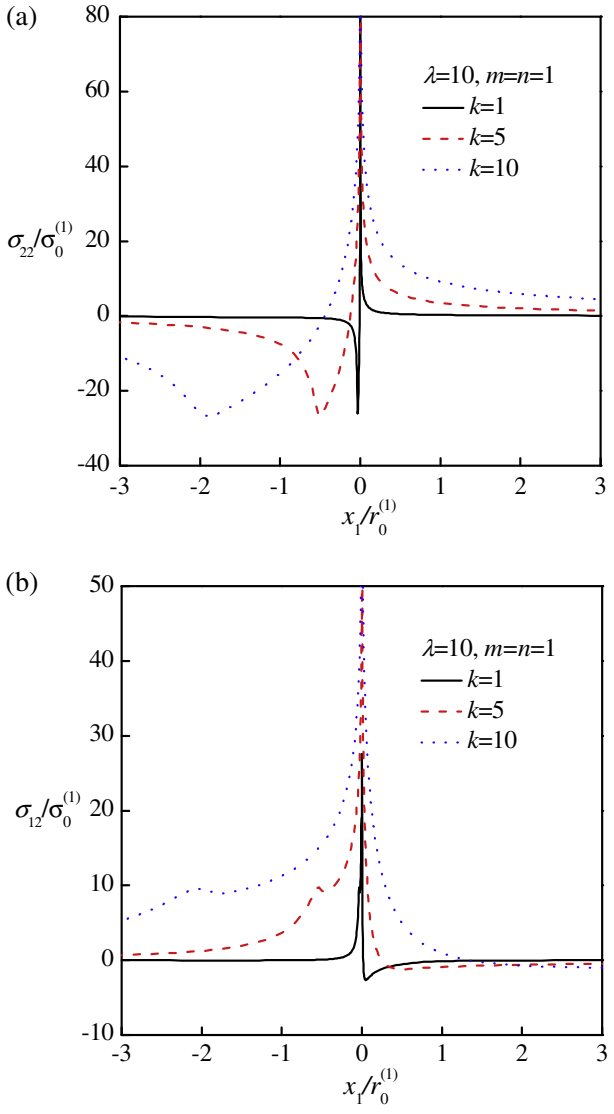

Fig. 7. The variation of normalized stress fields with k for the case of $\lambda = 10$ and $m = n = 1$. (a) Normal stress σ_{22}. (b) Shear stress σ_{12}.

of the electrode have logarithmic singularity in a homogeneous electrostrictive material. The numerical solution of the near-tip fields follows the logarithmic singularity. We investigate the singular stress fields near the edge of the electrode for two types of the material property mismatches of dissimilar electrostrictive materials. First, the stress fields are computed for the combination of dissimilar electrostrictive materials with only the electrical mismatch. The variation of the normal stress field and the shear stress field along the x_1-axis at $x_2 = 0$ with λ, when $k = m = n = 1$, is shown in Fig. 6. The compressive stress behind the edge of an electrode is stronger and the tensile stress ahead of the edge increases with λ. The shear stress field increases behind the edge of an electrode, but increases ahead of the edge of an electrode. Fig. 7 illustrates the variation of the stress components with k, when $\lambda = 10$ and $m = n = 1$. As k increases, the range of the compressive stress fields behind the edge of an electrode becomes larger, but the maximum absolute value of the normal stress is almost invariant. The strength of the tensile stress field ahead of the edge of an electrode is also greater as k increases. The shear stress field rapidly increases in the vicinity of the edge of an electrode as k increases. This result is at variance with that in Fig. 6. The variation of stress components with n for the case when $k = \lambda = m = 1$ is shown in Fig. 8. The compressive stress field behind the edge of an electrode increases as n increases. The compressive stress field is approximately maximized at the location of $x_1/r_0^{(1)} = -2$ regardless of the increment of n. The tensile stress field ahead of the edge of an electrode increases with n. The shear stress field rapidly increases both behind and ahead of the edge of an electrode. Second, we consider the stress fields for the case with only the elastic mismatch. The variation of the stress components with m, when $k = \lambda = n = 1$, is shown in Fig. 9. The shape of the plots of the compressive and tensile stress fields near the edge of an electrode is similar to those in Fig. 8. However, the rate of increment of the normal stress fields decreases as m increases.

5. Crack initiation

Near the edge of an electrode, the incompatible strains are induced by the non-uniform and the intensive electric fields; thereby, the strong stress is generated for satisfying the compatibility condition. The hoop stress ahead of the electrode edge is tensile, therefore, the small crack is readily nucleated in the material

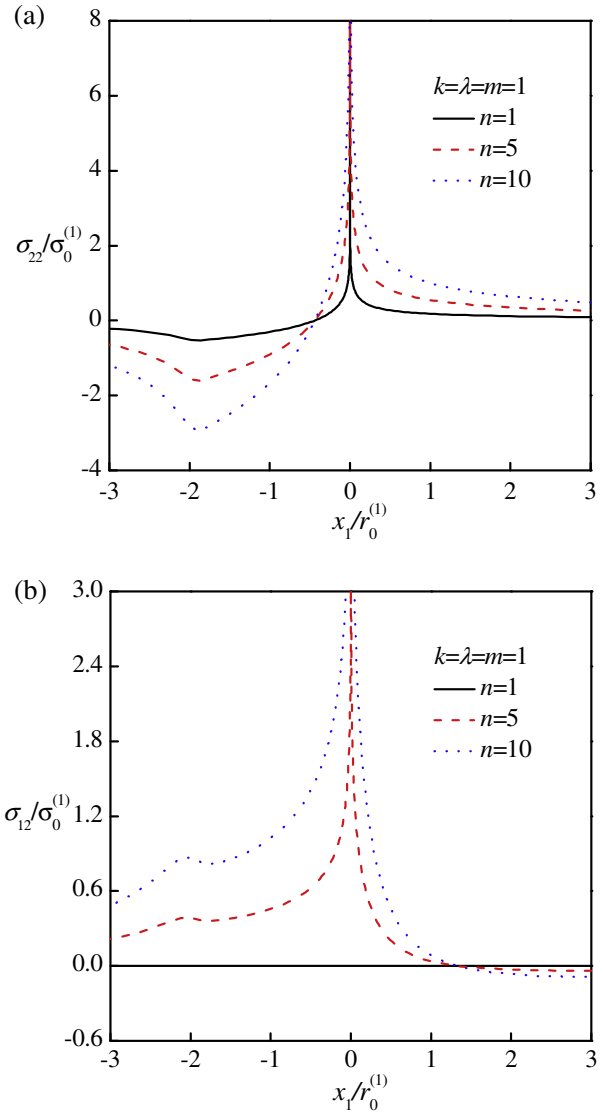

Fig. 8. The variation of normalized stress fields with n for the case of $k = \lambda = m = 1$. (a) Normal stress σ_{22}. (b) Shear stress σ_{12}.

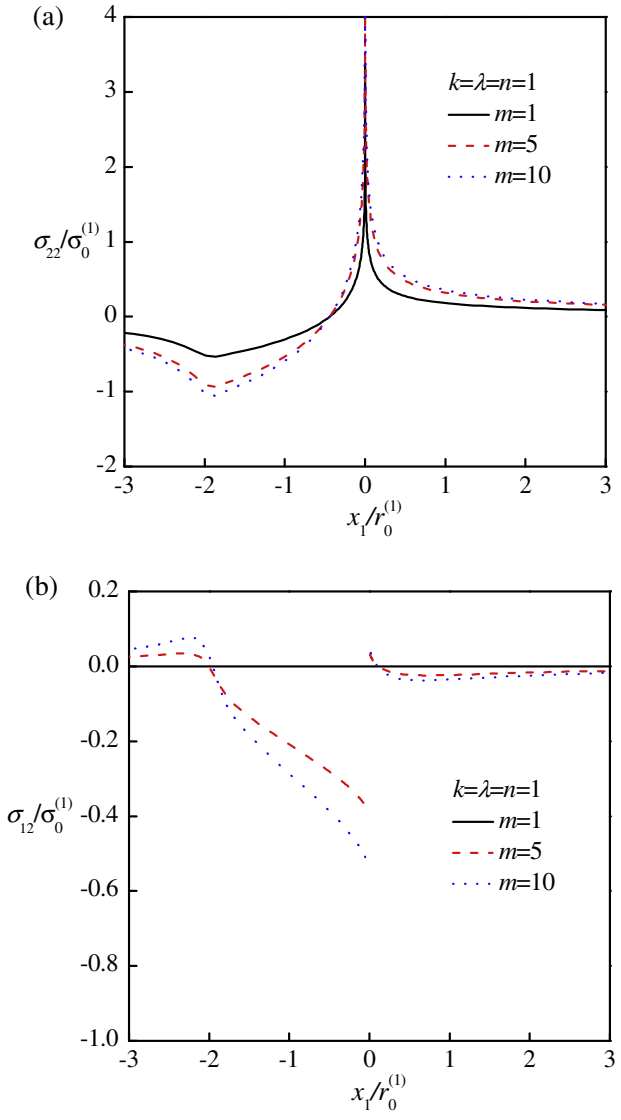

Fig. 9. The variation of normalized stress fields with m for the case of $k = \lambda = n = 1$. (a) Normal stress σ_{22}. (b) Shear stress σ_{12}.

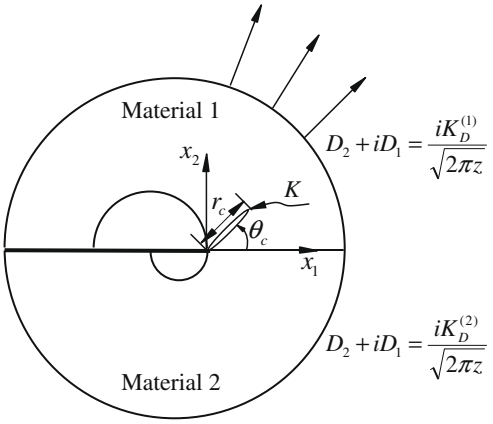

Fig. 10. Crack initiated from a semi-infinite electrode.

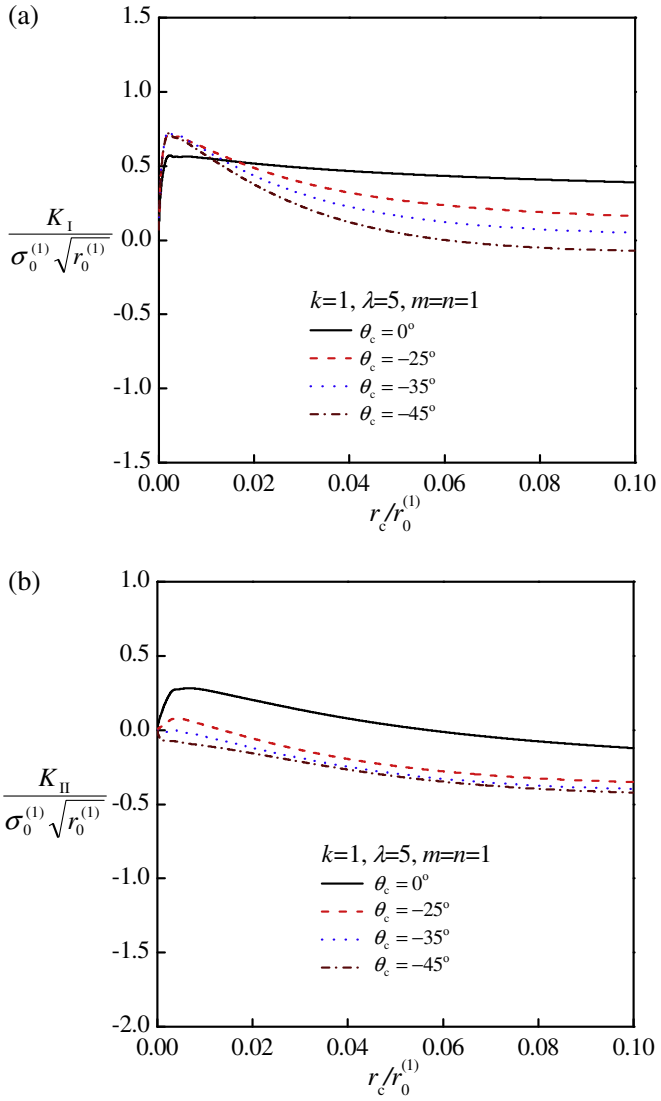

Fig. 11. Normalized stress intensity factors as functions of r_c when k = 1, λ = 5, and m = n = 1. (a) Mode I. (b) Mode II.

ahead of the electrode edge. According to Hao et al. (1996), the cracks nucleated extend into the medium by the following physical processes. First of all, the conducting species released from the metal electrode migrate on the crack surfaces. Then, the crack behaves just as the newly created electrode and the electric fields around the crack tip become non-uniform and magnified. Again, the stress fields are concentrated near the crack tip and extend the crack.

Consider the small crack that is initiated from the edge of a semi-infinite electrode, as shown in Fig. 10. The small crack has the length r_c and lies in the direction of the angle θ_c to the positive x_1-axis. The surfaces of the small crack are assumed to be electrically permeable because the gap between the surfaces of the small crack is very narrow. Hence, the electric displacement fields near the edge of the electrode are not disturbed by the cracking. Since the stress fields are asymmetric with respect to the interface, the orientation of the small crack will deviate from the direction of the interface. The surfaces of the small crack are traction-free. The electric potentials on the surfaces of the small crack are assumed to be zero. Hence, the surface conditions of the small crack are given by the forms

$$\begin{aligned} &\phi^+(r,\theta_c) = \phi^-(r,\theta_c) = 0, \\ &\sigma_{ij}^+(r,\theta_c) = \sigma_{ij}^-(r,\theta_c) = 0 \quad \text{for } 0 < r < r_c. \end{aligned} \tag{12}$$

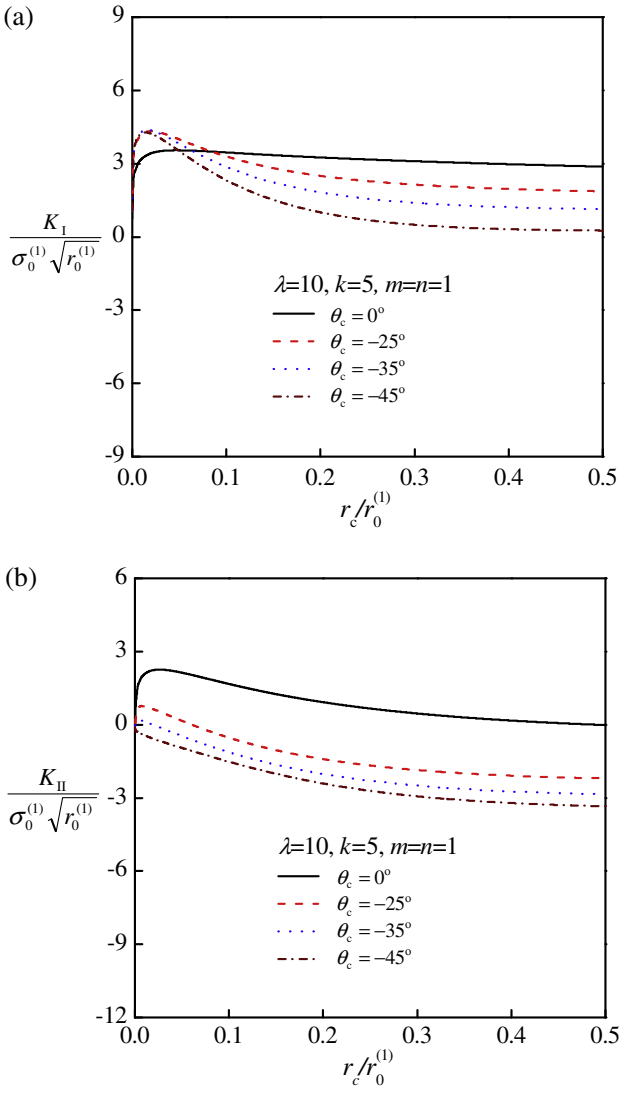

Fig. 12. Normalized stress intensity factors as functions of r_c when λ = 10, k = 5, and m = n = 1. (a) Mode I. (b) Mode II.

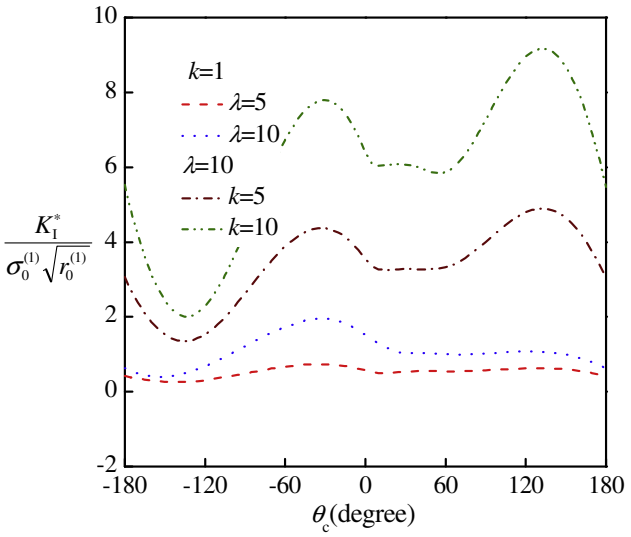

Fig. 13. K_I^* as a function of θ_c for various combinations of k and λ.

The complex interface stress intensity factor $K = K_1 + iK_2$ is given by (Suo, 1989)

$$K = \sqrt{\frac{2}{\pi}}\cosh \pi\mu (r_c)^{-1/2-i\mu} \int_0^{r_c} (\sigma_{\theta\theta} + i\sigma_{r\theta}) \left(\frac{r}{r_c - r}\right)^{1/2+i\mu} dr, \quad (13)$$

μ is the oscillatory index given by

$$\mu = \frac{1}{2\pi} \ln\left(\frac{1-\beta}{1+\beta}\right). \quad (14)$$

Here, $\beta = [(1-2\nu)(1-m)]/[2(1-\nu)(1+m)]$ because $\nu^{(1)} = \nu^{(2)}$. If $\beta = 0$, the interface stress intensity factor becomes the conventional stress intensity factor $K = K_I + iK_{II}$, where K_I and K_{II} are the Mode I and Mode II stress intensity factors. $\sigma_{\theta\theta}$ and $\sigma_{r\theta}$ are obtained through numerical stress analysis.

Through dimensional consideration, the complex interface stress intensity factor at the tip of the crack is expressed as

$$K\left(r_0^{(1)}\right)^{i\mu} = \sigma_0^{(1)}\sqrt{r_0^{(1)}}\Lambda(k, \lambda, m, n, \nu, q), \quad (15)$$

In Eq. (15), Λ is the dimensionless complex interface stress intensity factor given by $\Lambda = \Lambda_1 + i\Lambda_2$. For the case when $k = 1$, $\lambda = 5$, and $m = n = 1$ as well as for the case when $\lambda = 10$, $k = 5$, and $m = n = 1$, the normalized stress intensity factors as a function of r_c are shown in Figs. 11 and 12. For a given θ_c, the stress intensity factor of Mode I has a peak value (K_I^*) when $r_c = r_c^*$. The distance r_c^* that corresponds to the maximum stress intensity factor varies withθ_c. In Fig. 13, K_I^* is plotted as a function of θ_c for various combinations of k and λ. K_I^* has the maximum value at $\theta_c \approx -30°$ in material 2 and at $\theta_c \approx 125°$ in material 1, respectively. Fig. 14 illustrates the normalized stress intensity factors as functions of r_c for the case when $n = 5$ and $\lambda = k = m = 1$. It is seen from Fig. 15 that K_I^* has the maximum value at $\theta_c \approx -25°$ in material 2 and at $\theta_c \approx 135°$ in material 1, respectively. Also, Fig. 16 illustrates the normalized stress intensity factors as functions of r_c for the case when $m = 5$ and $\lambda = k = n = 1$. As shown in Fig. 17, K_I^* has the maximum value at $\theta_c \approx -105°$ in material 2 and at $\theta_c \approx 5°$ in material 1, respectively. When the small crack advances along the interface, the normalized stress intensity factors as functions of r_c for the case when $m = 5$ and $m = 10$ (and $\lambda = k = n = 1$) are shown in Fig. 18. As observed in Fig. 18, for the case when $m = 5$, Λ_1 has the maximum value, $\Lambda_1^* = 0.22$ when $r_0^* = 0.34r_0^{(1)}$. For the case when $m = 10$, the value of Λ_1 is maximized as $\Lambda_1^* = 0.247$ when $r_0^* = 0.39r_0^{(1)}$.

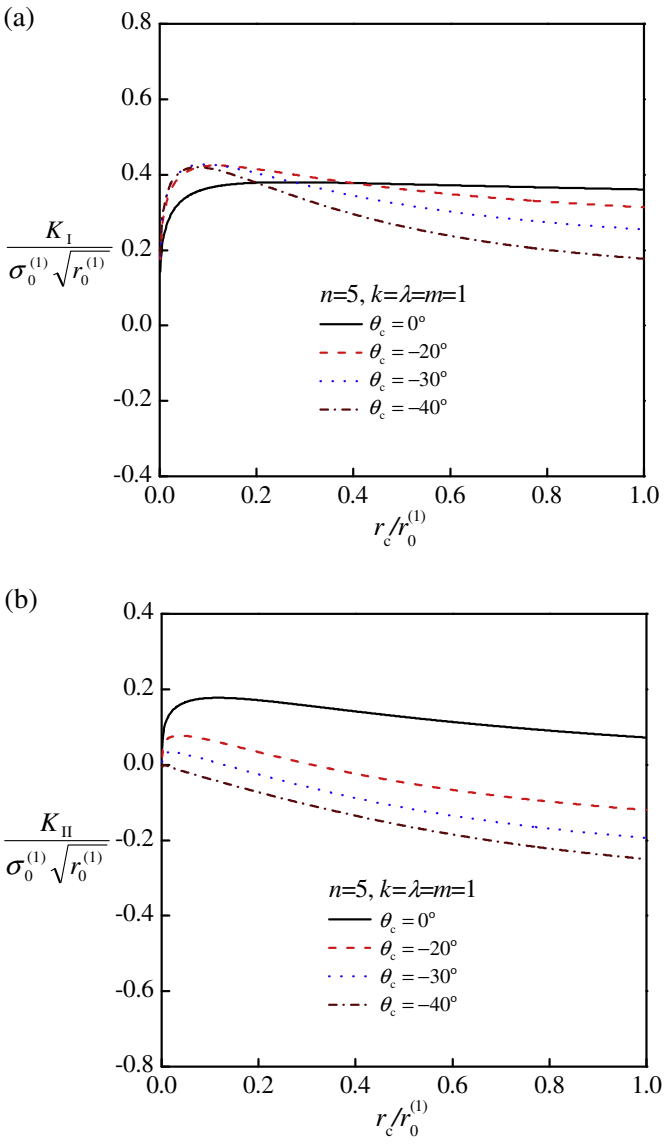

Fig. 14. Normalized stress intensity factors as functions of r_c when $n = 5$ and $k = \lambda = m = 1$. (a) Mode I. (b) Mode II.

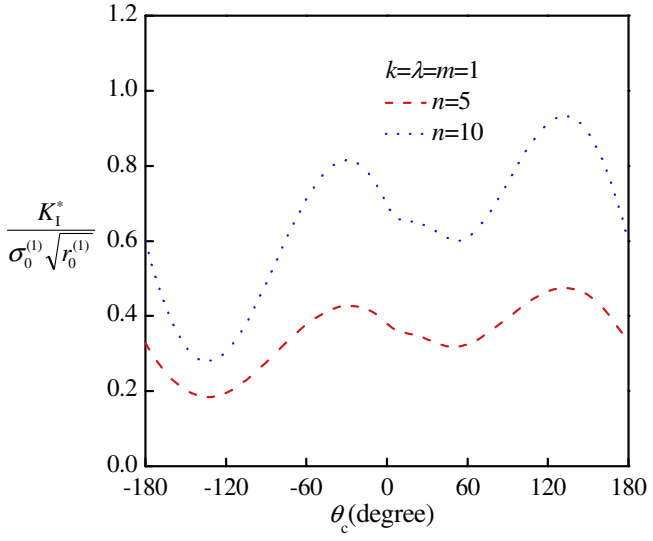

Fig. 15. K_I^* as a function of θ_c for various values of n.

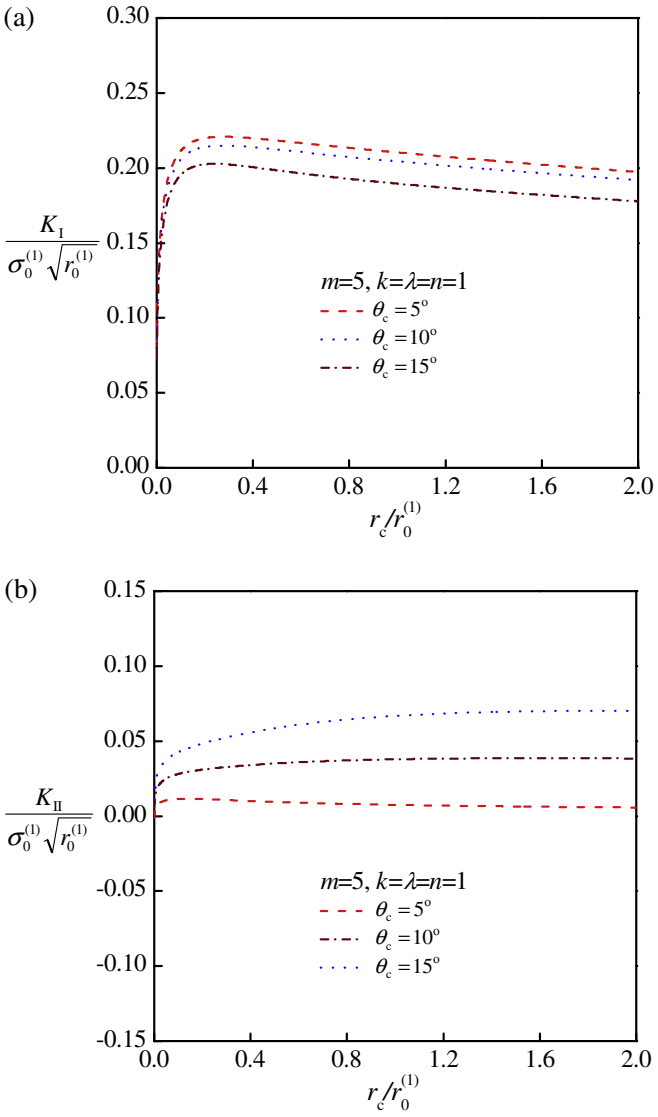

Fig. 16. Normalized stress intensity factors as functions of r_c when $m = 5$ and $k = \lambda = n = 1$. (a) Mode I. (b) Mode II.

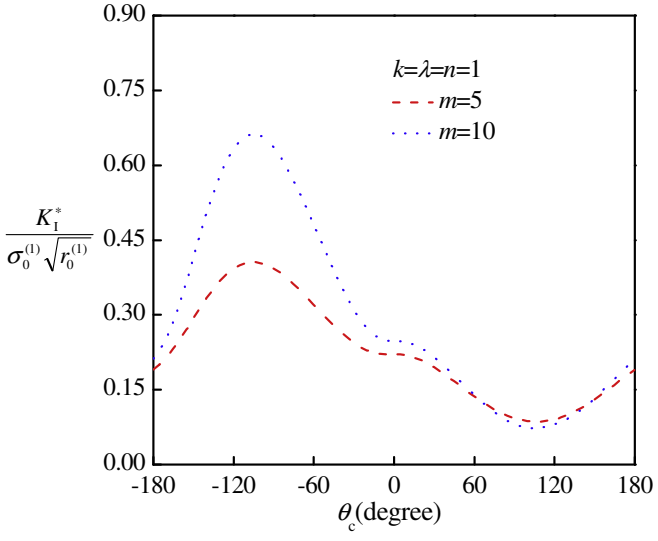

Fig. 17. K_I^* as a function of θ_c for various values of m.

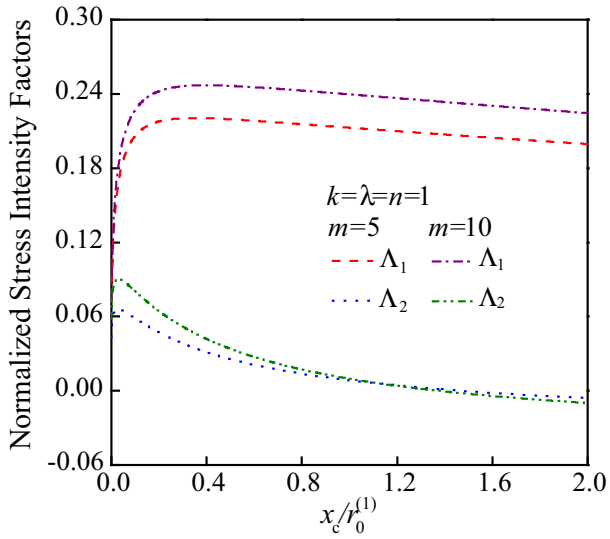

Fig. 18. Normalized stress intensity factors as functions of x_c for various m.

6. Conclusions

The asymptotic problem of a semi-infinite electrode between dissimilar electrostrictive materials is analyzed by the finite element method. The problem assumes the small-scale saturation condition. The numerical results of the electric displacement fields are obtained through electrostatic analysis on the basis of the mathematical equivalence between a Mode III problem and an electrostatic problem. It is shown that the ratios of the permittivities and the saturated electric displacements between dissimilar electrostrictive materials have an important effect on the shape and size of the saturation zone. Through the elastic analysis with the numerical solution of the electric displacement fields, the stress fields are obtained for various combinations of the material properties. The stress intensity factors for the small crack initiated from the edge of the electrode are obtained by the numerical integration of the stress fields. The effects of the electrostatic, elastic, and electrostrictive properties on the stress intensity factors are discussed.

Acknowledgement

This work was supported by Inha University Research Grant.

References

Aburatani, H., Harada, S., Uchino, K., Furuta, A., Fuda, Y., 1994. Destruction mechanisms in ceramic multilayer actuators. Japanese Journal of Applied Physics 33 (5B), 3091–3094.

Beom, H.G., 1999. Small scale nonlinear analysis of electrostrictive crack problems. Journal of the Mechanics and Physics of Solids 47 (6), 1379–1395.

Beom, H.G., Atluri, S.N., 2003. Effect of electric fields on fracture behavior of ferroelectric ceramics. Journal of the Mechanics and Physics of Solids 51 (6), 1107–1125.

Beom, H.G., Kim, Y.H., Cho, C., Kim, C.B., 2006. Asymptotic analysis of an impermeable crack in an electrostrictive material subjected to electric loading. International Journal of Solids and Structures 43 (22-23), 6869–6886.

Beom, H.G., Kim, Y.H., Cho, C., Kim, C.B., 2008. Modified boundary layer analysis of an electrode in an electrostrictive material. Archive of Applied Mechanics 78 (3), 191–209.

Gao, H., Zhang, T.-Y., Tong, P., 1997. Local and global energy release rates for an electrically yielded crack in a piezoelectric ceramic. Journal of the Mechanics and Physics of Solids 45 (4), 491–510.

Gong, X., Suo, Z., 1996. Reliability of ceramic multilayer actuators: a nonlinear finite element simulation. Journal of the Mechanics and Physics of Solids 44 (5), 751–769.

Hao, T.H., Gong, X., Suo, Z., 1996. Fracture mechanics for the design of ceramic multilayer actuators. Journal of the Mechanics and Physics of Solids 44 (1), 23–48.
Hom, C.L., Shankar, N., 1996. A finite element method for electrostrictive ceramic devices. International Journal of Solids and Structures 33 (12), 1757–1779.
Li, Q., Chen, Y.H., 2007. Solution for a semi-permeable interface crack between two dissimilar piezoelectric materials. Journal of Applied Mechanics 2007 (74), 833–844.
Li, Q., Chen, Y.H., 2008. Solution for a semi-permeable interface crack between elastic dielectric/piezoelectric bimaterials. Journal of Applied Mechanics (75). 011010-1 – 011010-13.
Ru, C.Q., Mao, X., Epstein, M., 1998. Electric-field induced interfacial cracking in multilayer electrostrictive actuators. Journal of the Mechanics and Physics of Solids 46 (8), 1301–1318.
Suo, Z., 1989. Singularities interacting with interfaces and cracks. International Journal of Solids and Structures 25 (10), 1133–1142.
Winzer, S.R., Shankar, N., Ritter, A.P., 1989. Designing cofired multilayer electrostrictive actuators for reliability. Journal of the American Ceramic Society 72 (12), 2246–2257.
Yang, W., Suo, Z., 1994. Cracking in ceramic actuators caused by electrostriction. Journal of the Mechanics and Physics of Solids 42 (4), 649–663.